Since January 2020 Elsevier has created a COVID-19 resource centre with free information in English and Mandarin on the novel coronavirus COVID-19. The COVID-19 resource centre is hosted on Elsevier Connect, the company's public news and information website.

Sensors & Actuators: B. Chemical 348 (2021) 130706

Contents lists available at ScienceDirect

Sensors and Actuators: B. Chemical

journal homepage: www.elsevier.com/locate/snb

SERS-based lateral flow immunoassay for sensitive and simultaneous detection of anti-SARS-CoV-2 IgM and IgG antibodies by using gap-enhanced Raman nanotags

Shiliang Chen [a,1], Liuwei Meng [a,b,1], Litong Wang [b], Xixi Huang [a], Shujat Ali [a], Xiaojing Chen [a,*], Mingen Yu [b], Ming Yi [b], Limin Li [a], Xi Chen [a], Leiming Yuan [a], Wen Shi [a], Guangzao Huang [a]

[a] College of Electrical and Electronic Engineering, Wenzhou University, Wenzhou 325035, PR China
[b] Research and Development Department, Hangzhou Goodhere Biotechnology Co.,Ltd., Hangzhou 311100, PR China

ARTICLE INFO

Keywords:
Lateral flow immunoassay
Gap-enhanced Raman nanotags (GERTs)
Surface-enhanced Raman scattering (SERS)
COVID-19
SARS-CoV-2
IgM/IgG

ABSTRACT

The lateral flow immunoassay (LFIA) has played a crucial role in early diagnosis during the current COVID-19 pandemic owing to its simplicity, speed and affordability for coronavirus antibody detection. However, the sensitivity of the commercially available LFIAs needs to be improved to better prevent the spread of the infection. Here, we developed an ultra-sensitive surface-enhanced Raman scattering-based lateral flow immunoassay (SERS-based LFIA) strip for simultaneous detection of anti-SARS-CoV-2 IgM and IgG by using gap-enhanced Raman nanotags (GERTs). The GERTs with a 1 nm gap between the core and shell were used to produce the "hot spots", which provided about 30-fold enhancement as compared to conventional nanotags. The COVID-19 recombinant antigens were conjugated on GERTs surfaces and replaced the traditional colloidal gold for the Raman sensitive detection of human IgM and IgG. The LODs of IgM and IgG were found to be 1 ng/mL and 0.1 ng/mL (about 100 times decrease was observed as compared to commercially available LFIA strips), respectively. Moreover, under the condition of common nano-surface antigen, precise SERS signals proved the unreliability of quantitation because of the interference effect of IgM on IgG.

1. Introduction

The novel coronavirus (COVID-19) pandemic has infected more than one hundred million people and caused millions of deaths. Early in vitro diagnosis of infectious diseases has been regarded as an effective anti-transmission measure because it can reduce the spread of viruses and guide prompt treatment [1,2]. Currently, the methods used to diagnose COVID-19 mainly include nucleic acid detection based on real-time PCR technology [3,4] and immunoglobulin detection based on immunological assays [5–7]. The former method has the advantages of high sensitivity and excellent accuracy. However, due to complex procedures and expensive instruments, it is difficult to implement the method in countries or areas with limited resources. Methods such as lateral flow immunoassay (LFIA) use a ubiquitous kit that offers the advantages of simplicity, inexpensiveness and flexibility, and meet the rapid screening requirements [8,9].

An LFIA strip (based on immune-strips and gold (Au) colloids) is considered to be the most prevalent rapid screening method [10–12], which can generate valuable data on the dynamics of virus infection and early diagnosing [2]. The main principle of the method is the determinants bind to the labelled antibodies (Au colloids) and move through capillary action until they are captured by the immobilized antibodies in the designated zone. Then, they exhibit colour that can be analysed by naked eye or other optical devices. However, it is difficult to provide any guarantee of the accuracy, sensitivity and quantification ability achieved by colorimetric recognition [13]. Recently, some LFIA biosensors have been developed for anti-SARS-CoV-2 antibodies detection. For example, Wang et al. have used Selenium nanoparticles instead of conventional Au colloid and obtained a good sensitivity to IgM (but not to IgG) [14], Liu et al. have adopted dual-layers DTNB-modified SiO_2@Ag NPs as SERS nanotags and obtained up to 800 times improvement as compared with colorimetric results [15] and Bayin et al. have used superparamagnetic nanoparticles (SMNPs) to reduce the detection limit to ng/mL level through a giant magnetoresistance (GMR)

* Corresponding author.
E-mail address: chenxj@wzu.edu.cn (X. Chen).
[1] Shiliang Chen and Liuwei Meng contributed equally to this work.

https://doi.org/10.1016/j.snb.2021.130706
Received 13 March 2021; Received in revised form 9 August 2021; Accepted 31 August 2021
Available online 3 September 2021

sensing system [16]. Similarly, dual-mode SiO2@Au@QD nanobeads, lanthanide-doped polystyrene nanoparticles and PS@QDs@SiO_2 nanobeads have been applied as fluorescent labels for analysis of clinical samples [17–19]. Especially, SERS nanotags, which provide very intense fingerprint signals, can be used in place of colorimetry and other sensors as an ultrasensitive indicator [20–22]. In recent years, SERS-based analytical technology combined with LFIA detection platform has attracted wide attention for trace biochemical detection of viruses [23, 24], bacteria [25,26], biomarkers [27–32] and harmful substances [33].

SERS nanotags usually consist of noble metal nanoparticles which serve as plasmon resonance enhanced substrates, and Raman-active molecules adsorb on or close to the nanoparticle surface. Here, we utilized a highly efficient SERS probe structure in which the Raman reporters were embedded in the interior-nanogap between the core and shell of the Au nanostructure [34,35]. This multilayer nanostructure, also called gap-enhanced Raman tags (GERTs) or nanomatryoshkas [34, 36,37], protect Raman reporters from external influences and minimize the effects of desorption. Furthermore, GERTs provide a large electromagnetic (EM) field generated by the plasmons coupled between both sides of the gap, result in more than one order of magnitude enhancement compared with conventional nanotags [34,38]. In addition to SERS-based LFIA, this nanotag has been used in various sensors research such as dot-immunoassay [39,40], cell imaging [37,41–43] and unclonable anti-counterfeiting labels [44]. To ensure the generation of outstanding Raman signals, 4-nitrobenzenethiol (4-NBT), which exhibits the largest Raman cross-section among thiol aromatic derivatives, was selected as a Raman reporter [27,45] and spacer. IgM and IgG were conjugated with immune-sensing probes and immobilized on the corresponding test lines. Then, they were identified via colorimetric assays and Raman spectrometer.

The viral infection usually results in the production of IgM, followed by the production of IgG in several weeks. Hence, simultaneous detection of IgM and IgG will provide more information about the stage of infection in positive patients. Therefore, the SERS-based LFIA strips were used to develop an in vitro diagnostic (IVD) and point-of-care (POC) method which offers the advantages of speed, sensitivity and multiplex detection of IgM and IgG. In this study, not only the detection sensitivity was discussed (compared with commercially available LFIA strips and other improved LFIA strips), but also the quantitative feasibility and critical comparison with other improved LFIA strips were carried out. In view of this, the work will provide a new perspective for the sensitive multiplex detection of biomarkers or viruses in current and future pandemics.

2. Experimental section

2.1. Materials and chemicals

Chloroauric acid tetrahydrate ($HAuCl_4{\cdot}3H_2O$) was purchased from Shanghai Anpel Reagent (Shanghai, China). Ascorbic acid, cetyltrimethylammonium chloride (CTAC), 4-NBT, trisodium citrate, sodium hydroxide (NaOH), Tris (hydroxymethyl) aminomethane, hemoglobin (HB) and triglyceride (TG) were obtained from Maclink Reagent (Beijin, China). Bilirubin sodium (BIL) was purchased from J&K Scientific (Beijing, China). A 0.5 M phosphate-buffered saline (PBS, pH 7.6) solution was used to control pH. A 50 mM Tris solution containing 1% Tween-20% and 1% bovine serum albumin (BSA) was used as the dilution buffer. All of the aqueous solutions were prepared in ultrapure water that was purified with a Millipore Milli-Q system (18.24 MΩ/cm). The nitro-cellulose (NC) membrane (Sartorious CN140 with 8 μm pore size), Millipore glass fibre conjugated pad, absorbent pad and sample pad (Ahlstrom 8964) were obtained from Joey-bio (Shanghai, China). Commercial anti-SARS-CoV-2 IgM/IgG detection LFIA strips, COVID-19 recombinant antigens (CN97), positive standard IgM and IgG, mouse anti-human IgM and IgG, chicken IgY and goat anti-chicken IgY were supplied by Hanzhou Goodhere Biotechnology Co. (Hanzhou, China).

2.2. Instrumentation

High-resolution TEM images were obtained with a JEM-2100F electron microscope at an accelerating voltage of 200 kV. Scanning electron microscopy (SEM) images were taken by an FEI Nova 200 NanoSEM instrument operated at 20 kV. UV–vis extinction spectra of nanoparticles were measured with a Shimadzu UV-2650 spectrometer. SERS mappings of SERS-based LFIA strips were acquired on a Renishaw inVia Plus Raman system (785 nm laser). A Leica optical microscope and an Olympus 20× objective lens were used to focus a 10 μm diameter spot and the illumination area inside the test zone was 290 × 390 μm (1131 pixels). The laser power was set to 5% (15 mW) and the acquisition time was 1 s per step size. The obtained spectra were modified by baseline subtraction and smoothed via Renishaw WiRE4.2. Three random tests were performed on each test line for each sample. The SERS signals of the NBT-Au and GERT solutions were detected by an Optosky ATR3110 portable Raman spectrometer supplied by Xiamen Optosky Technology Co. (Xiamen, China).

2.3. Preparation of GERTs

Gold nanoparticles with a diameter of 55 nm (cores of the nanotags) were prepared according to a previous report with slight modifications [46]. Typically, 0.35 mL of trisodium citrate solution (1% wt) was added to 49.5 mL of a boiling $HAuCl_4$ aqueous solution (0.01% wt) and stirred for 30 min. Then, 0.5 mL of trisodium citrate (1% wt) was added and stirred for 2 min. The reaction mixture was cooled to room temperature, which yielded red-purple Au nanoparticles. Next, 500 μL of 250 mM CTAC solution containing 25 μg/mL 4-NBT was added to 2 mL of the above Au core nanoparticles under vigorous stirring at room temperature for 30 min. These modified Au cores were centrifuged twice at 10, 000 rpm for 3 min to discard the unabsorbed molecules with CTAC (50 mM), and then, the modified Au cores were resuspended in 50 mM CTAC. The Au shells of the nanotags were grown by adding 20 mL of CTAC solution (50 mM), 200 μL of aqueous $HAuCl_4$ (1% wt) and 480 μL freshly prepared ascorbic acid solution (50 mM) to 2.5 mL of the pre-formed cores. The mixture was stirred at room temperature for 30 min, the colour of the solution changed from the initial light red to blue-grey and orange-red. The final product was washed twice with trisodium citrate solution (0.01% wt) by centrifugation at 10,000 rpm for 3 min and dispersed in the same volume of trisodium citrate solution (0.01% wt).

2.4. Preparation of immune-GERTs and immune-Au

Immune-GERTs were functionalized with COVID-19 recombinant antigens (CN97) obtained by the combination of coronavirus spiked-protein (S-protein) and nucleocapsid protein (N-protein) through a sequence of amino acids (GGGGSGGGGSGGGGS) as a soft linker. The soft linker structure keeps S-protein and N-protein separately, assist in free rotation and avoid interfering with each other.

First, 20 mL of nanotag solution was taken and the pH was adjusted to 8.0 with PBS (0.5 M) and NaOH (1 mM). Then, 200 μL of recombinant antigen (1.1 mg/mL) was added under stirring (600 rpm) for 1 h to obtain conjugates through electrostatic adsorption. Subsequently, the conjugates were blocked with 200 μL of 10% BSA under stirring (600 rpm) for 1 h. Finally, the above solution was centrifuged at 6000 rpm for 20 min to remove the uncoated biomolecules and then resuspended in 2 mL of Tris-HCl solution (10 mM, containing 1% BSA). All of the above processes were performed at room temperature. To realize independent quality control, Au nanoparticles (55 nm) were functionally modified with chicken IgY. The fabrication processes and reaction parameters were consistent with the above protocols used for Immune-GERT synthesis by using chicken IgY instead of recombinant antigen.

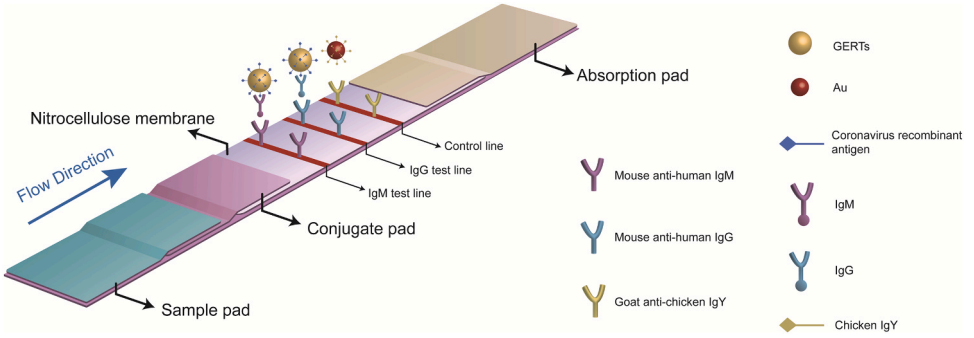

Fig. 1. Schematic diagram of the SERS-based strip for the detection of IgM and IgG.

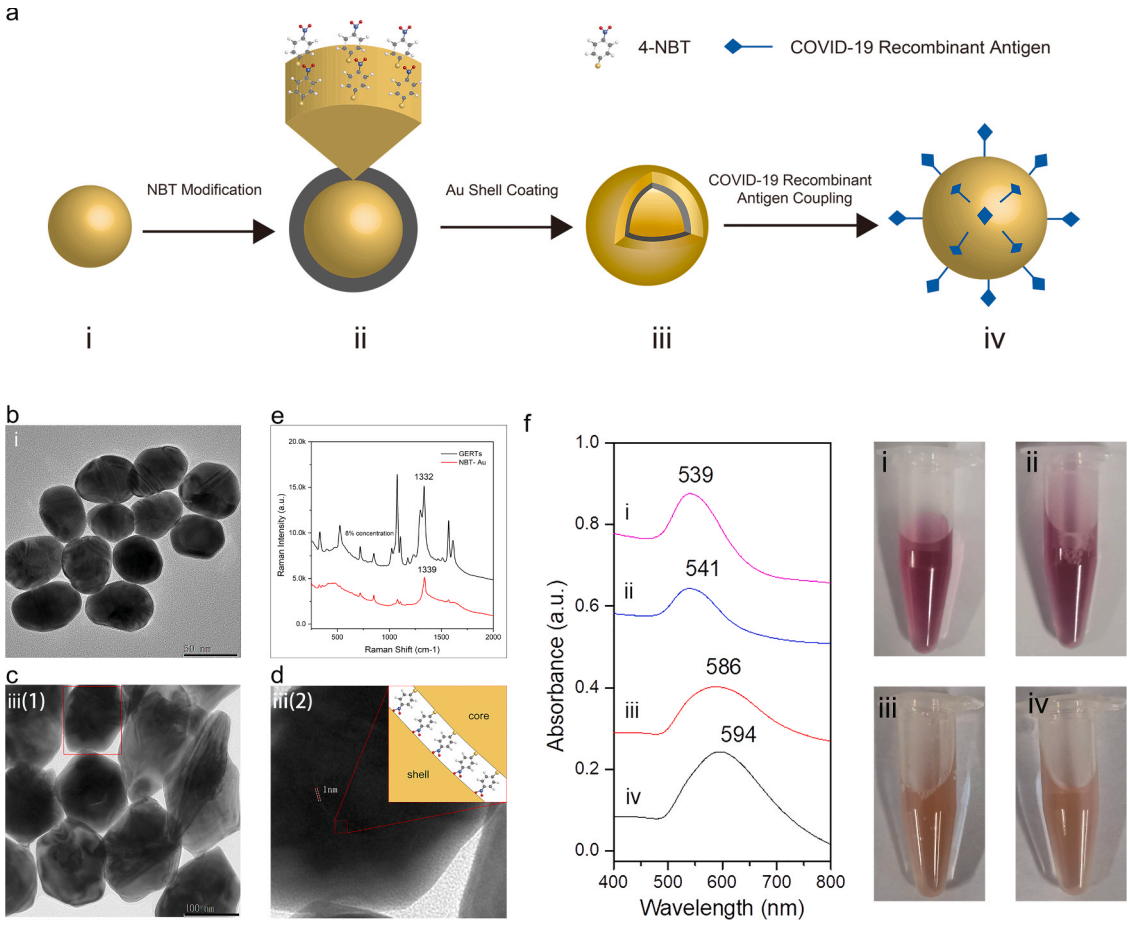

Fig. 2. (a) Scheme of GERTs and immune-GERTs synthesis. (b) TEM image of 55 ± 5 nm Au cores. (c, d) TEM image of GERTs and an enlarged image with a 1 nm gap between the Au core and shell. (e) SERS spectra of NBT-Au and GERTs. (f) UV–vis extinction spectra and photographs of the four steps of colloid synthesis.

2.5. Preparation of the SERS-based LFIA strip for IgM and IgG detection

The conditions for the preparation of SERS-based LFIA strips were optimized according to the commercial scheme of Hangzhou Goodhere Biotechnology Co. Fig. 1 shows a schematic diagram of the SERS-based LFIA strip. IgM and IgG test lines were separately coated on the surface of NC membrane by spraying mouse anti-human IgM (1 mg/mL) and IgG (1 mg/mL), and the control line was coated by spraying 0.5 mg/mL polyclonal goat anti-chicken IgY. In the above processes, 0.8 mm wide dispensing bands were formed on a fixed area of the NC film at a constant rate (0.1 μL/mm) through a line dispensing instrument (HMY300, Hanzhou Weizan Technology Co.). Subsequently, the prepared NC membrane was dried in an incubator at 37 ℃ for 1 h. The conjugate pad was prepared by spraying immune-nanoparticles onto a piece of glass fibre at a constant rate (4 μL/cm) via a high precision plane spray instrument (PJY200, Hanzhou Weizan Technology Co.). The immune-nanoparticles were premixed by immune-GERTs and immune-Au (3:1, 100 times concentrated). Then, the prepared conjugate pad was dried in an oven at 37 ℃ for 1 h. Finally, the as-prepared NC membrane, a conjugate pad, a sample pad and an absorption pad were assembled onto a plastic backing pad and then cut into individual 4 mm strips via an automatic guillotine cutter (QZY100, Hanzhou Weizan Technology Co.). The obtained strips were stored in a dry environment.

2.6. LFIA experiment

Before testing, all the solutions were warmed to room temperature. Then, 20 μL of serum (blood) sample was taken and diluted in 50 μL dilution buffer. This diluted sample was added to the sample pad, and the result was checked after 15 min. A colorimetric method was used followed by Raman spectroscopy for ultra-sensitive analysis. Due to the local epidemic prevention and control policy, it was very difficult to obtain clinical samples. Therefore, simulated samples were designed for analysis.

3. Results and discussion

3.1. GERTs synthesis and characterization

As shown in Fig. 2a, the preparation process of immune-GERTs was divided into three steps. (1) The modification of NBT on Au core surfaces, (2) Au shell growth and gap formation based on NBT-Au and (3) the functional modification of COVID-19 recombinant antigens on the GERTs surface.

The first step was different from the common scheme applied for the preparation of Au cores using a surfactant as a capping reagent [27,38,39,41,42,47]. The Frens method [48] was used to synthesize spherical cores with a particle size of ~55 ± 5 nm (Fig. 2b). As compared to previously reported Au cores with particle size less than 40 nm [39,41–43], the 55 nm Au cores have a stronger surface electromagnetic enhancement effect and thus achieved a stronger SERS signal [49]. However, bare Au cores with such large particle size were easy to aggregate during the molecular modification process. Hence, CTAC was added as a stabilizer to prevent aggregation. 4-NBT was used as reporter molecule because it exhibits the largest Raman scattering cross-section among thiol aromatic derivatives [27,45] and has excellent chemical affinity for Au. The adsorption of 4-NBT molecules on the Au core surface was a crucial factor for the formation of gap between the core and shell. Here, 4-NBT was used in excess (5 μg/mL) to saturate the core surface. The CTAC and 4-NBT were simultaneously added to the bare cores to ensure the rapid adsorption of 4-NBT on the Au surface without aggregation.

At present, there is still a debate about the effect of adsorption degree of 4-NBT molecules on shell formation. For instance, Zhang et al. have proposed that the formation of a smooth shell was affected by incubation time, which tended to form a “petal-like” shell [42]. Nevertheless, Khlebtsov et al. have reported that this was resulted from the extra 4-NBT molecules in the reaction solution [40]. Here in this work, to obtain a smooth shell for further surface modification, we investigated the adsorption degree of 4-NBT on the Au surface by using time-dependent SERS analysis. Figure S1a,b shows Raman spectra and intensity curves for the reaction time of 4-NBT incubated on Au cores. When 4-NBT was added, a signal of 1181 counts was observed within a few seconds, and then, the signal gradually increased to 2737 counts in 20 min. When the incubation time was 20–90 min, the SERS signal tended to be stable at approximately 2800–2900 counts. Further extension in the incubation time to 16 h slightly increased the signal to 3580 counts. Accordingly, three typical incubation times (2 min, 30 min and 16 h) were selected to coat the shells. As shown in Fig. S2a, when the incubation time was 2 min, no distinct core-shell morphology was observed, and instead, uniform spherical nanoparticles (having irregular gaps) with 120 ± 10 nm diameters were formed [34]. This is because the insufficiently adsorbed molecules (acting as spacers) were not enough to support the formation of a gap between the core and shell. Moreover, this structure was accompanied by a relatively poor Raman enhancement signal (Fig. S2b). On the other hand, GERTs with obvious interior nanogaps were obtained upon incubation for 30 min. Furthermore, GERTs with irregular morphology and obscure gaps were produced when incubated for 16 h (Fig. S2c), similar to previously reported flower-like structure [41,43]. We presumed that after long time incubation, some 4-NBT molecules on the surface of the cores dissociated and interfered with the regular coating, and led to anisotropic growth of the shell. Surprisingly, this structure has a stronger probe signal, approximately six times stronger than that of the former GERTs (Fig. S2d). However, the irregular surface was not favourable for antigen modification and couldn’t fulfilled the nanotag requirements for this study. Therefore, 30 min was selected as the optimal adsorption time to ensure the formation of a stable 4-NBT molecular layer on the 55 nm Au cores.

In the second stage, the Au shell was grown on the core surface by reducing chloroauric acid with ascorbic acid in the CTAC solution, and the NBT layer served as the Raman reporters and spacers. A typical overview of the GERTs is shown in Fig. 2c,d, which depicts the gap between the core and shell. The gap size was estimated to be 1 nm, which is in agreement with previous reports [27,45]. The morphology of the GERTs was polygonal, the nanoparticle size was approximately 140 ± 25 nm and the average Au layer thickness was approximately 40 nm. Some of the GERTs showed irregular shapes, this is because the presence of reporter molecules (layer) on the core surface affected the growth dynamics of the Au shell and the morphology of the GERTs. From an optical point of view (Fig. 2f), the colour of the GERTs solution was markedly different from that of the Au core solution and was changed from red to orange. Moreover, the SPR peak of the GERTs was shifted from 539 to 586 nm and broadened. This indicated an increase in non-uniform and large size particles. To further investigate the performance of the nanotags with gap structures, the SERS signals of the GERTs and NBT-Au were detected at identical excitation conditions (laser power, integration time and focal distance) by a portable Raman device. The concentration of the latter was 12.5 times that of the former, which was calculated based on the cores and synthesized product solution volume. For NBT-Au, the main characteristic peaks of NBT were 720, 849, 1077, and 1339 cm^{-1}, corresponded to π(CH) + π(CS) + π(CC), δ(CH), ν(CS) and ν(NO_2) vibrations, respectively. For the GERTs, the 4-NBT signals were significantly enhanced, and more characteristic peaks at 329, 528 and 1568 cm^{-1} were observed, corresponded to δ(CS), γ(CCC) and ν(CC) vibrations, respectively. In addition, the Raman shift of the ν(NO_2) vibration was shifted to 1332 cm^{-1}, reflected a change in the 4-NBT structure and reduction in the electron density of the nitro group influenced by the surface conductive Au shell. This was regarded as an important indicator that molecules were embedded in the interior nanogaps [50]. Here, the Raman shift was taken corresponded to the ν(NO_2) vibration with the strongest amplitude as the characteristic peak of 4-NBT for both nanoparticles. As shown in Fig. 2e, after the GERTs formation, the signal intensity was increased sharply from 2884 to 7028 counts. Based on the concentration ratio, an increase of approximately 30-fold was obtained.

In third stage, the immune-GERTs were obtained by functionalizing the GERTs surface with COVID-19 recombinant antigens, which were prepared by our group and used as a commercial product in the current pandemic. The following selected steps were applied to improve the commercial protocol. In brief, excess recombinant antigens (10 μg per 1.1×10^{-3} g GERTs) were attached to the GERTs surface by electrostatic interactions at the isoelectric point. The abundant amino groups randomly distributed on the antigen surface provided a strong affinity to Au and promoted the formation of a stable binding layer [51]. Then, excess BSA was used as a blocking agent to cover up the remaining free sites on the GERTs surface and prevent further nonspecific binding. From an optical point of view (Fig. 2f), the colour of the GERTs after functionalization with modified proteins did not change significantly, but an apparent redshift from 586 to 594 nm was observed in the extinction spectrum. This is due to the swollen corona of the surface protein micelles, which resulted in a larger hydration particle size for the GERTs. The synthesized immune-GERTs were used to fabricate a conjugate pad. The immune-GERTs were found stable and can be stored at room temperature for at least two months.

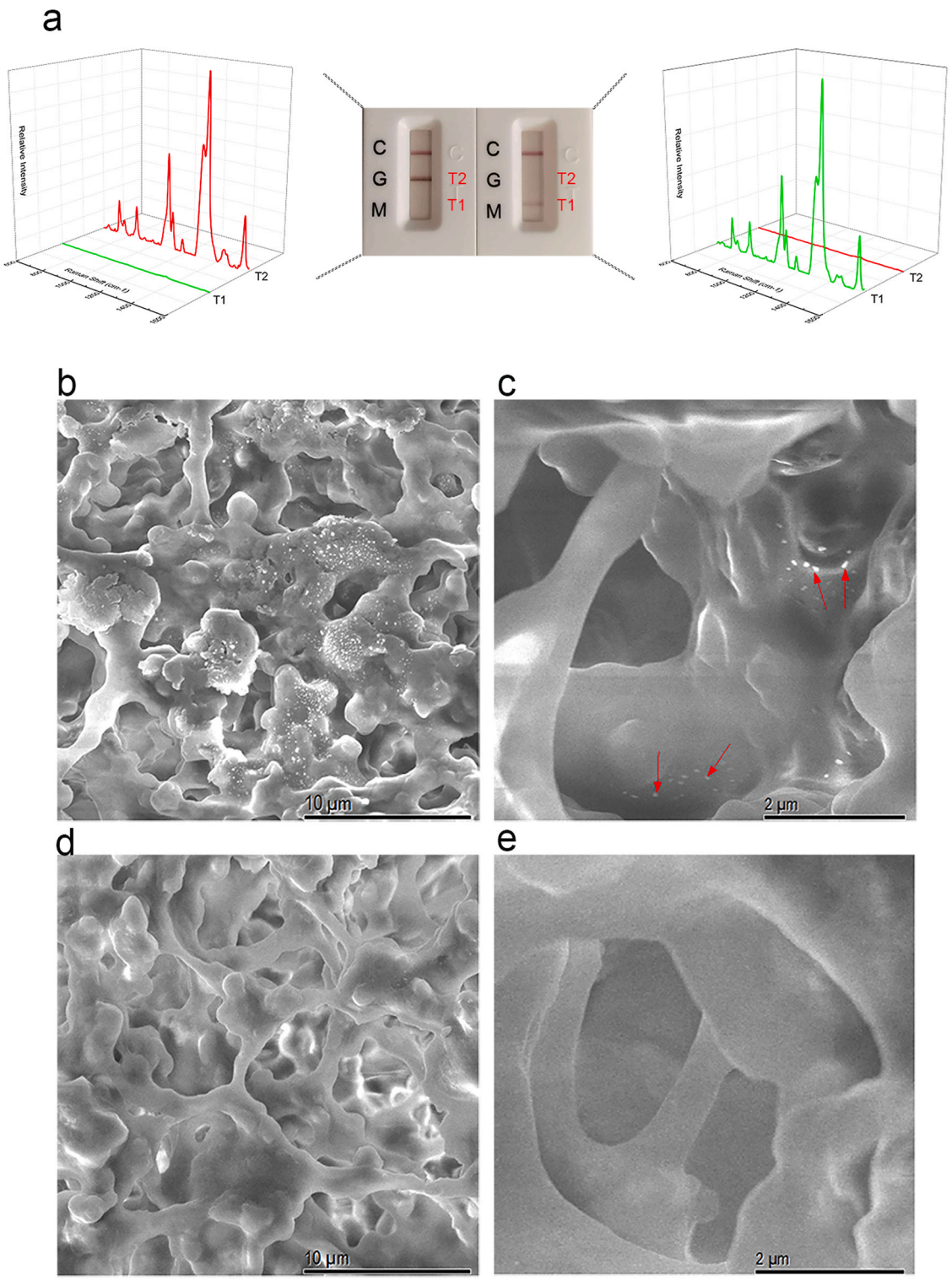

Fig. 3. (a) Photographs and corresponding SERS spectra of the test lines of the SERS-based strips in the presence of IgM and IgG. (b, c) Typical SEM images of the test zone for positive samples; the red arrows point to the nanoparticles of the positive sample in the enlarged image. (d, e) Typical SEM images of the test zone for negative samples.

3.2. The performance of SERS-based LFIA strips for anti-SARS-CoV-2 IgM and IgG detection

3.2.1. The principle of SERS-based LFIA strip

Figure 1 shows a schematic diagram of the SERS-based LFIA strip, which consists of a conventional LFIA strip and the SERS-based nanotag. As the blood/serum sample was added to the sample pad of the SERS-based LFIA strip, the liquid moved to the conjugate pad through capillary action, whereby a specific interaction occurred between the antibodies and coronavirus recombinant antigens on the GERT surface. Then, the above complexes moved to the NC membrane and migrated in the direction of the IgM test line (T1 line), IgG test line (T2 line) and control line (C line). In the presence of IgM or IgG, the corresponding conjugates were captured by the T1 or T2 line with goat anti-mouse IgM

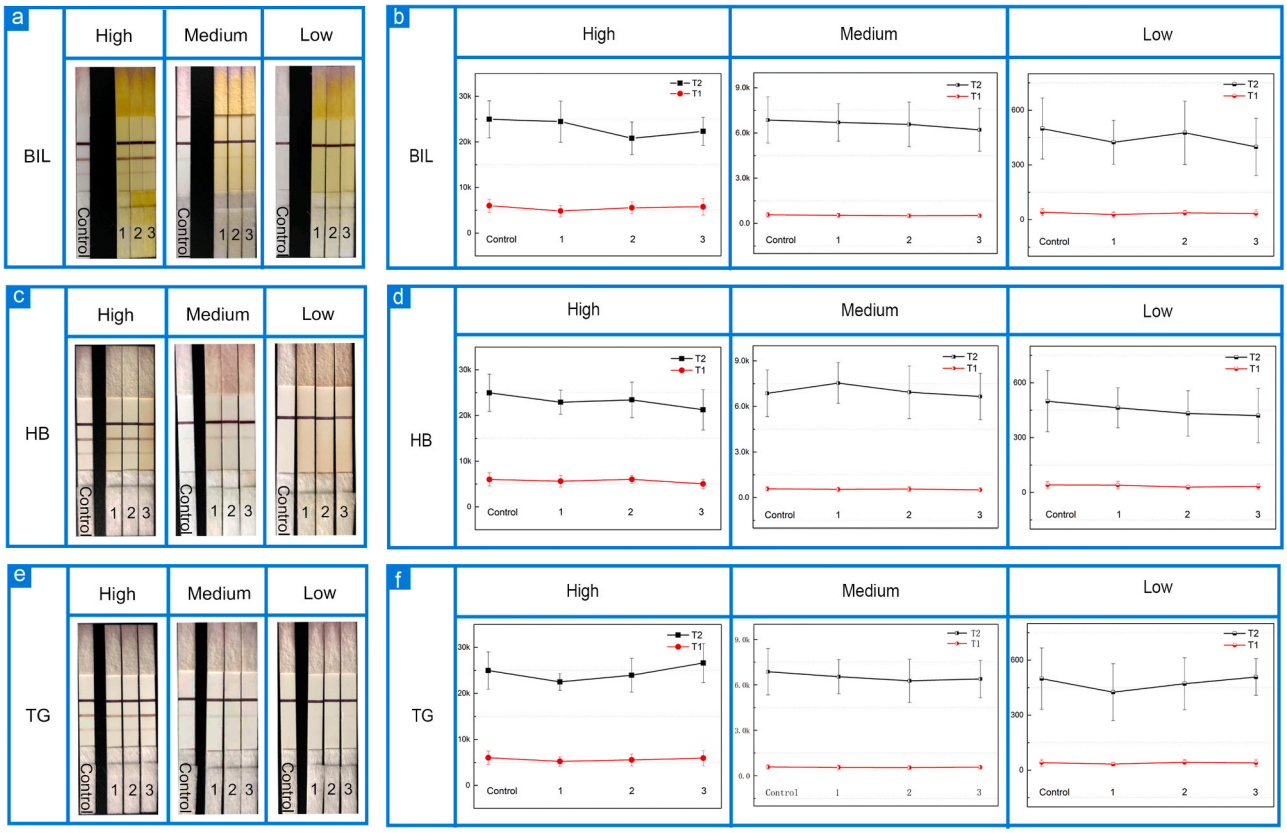

Fig. 4. Images of colorimetric results of different antibodies concentrations under the interference of BIL (a), HB (c) and TG (e). Corresponding Raman intensity of T1/T2 at different antibodies concentrations under the interference of BIL (b), HB (d) and TG (f). All error bars represent standard deviation ($n = 3$).

or IgG coating, respectively. Unlike the above-mentioned reports [14,15,17,18], the remaining objects that contain chicken IgY-modified Au moved on and were captured by the C line coated by goat anti-chicken IgY. This realized independent quality control and was not affected by T line combination. Moreover, this approach can effectively save the raw material (recombinant antigens) to increase yield, especially in the early stage of the epidemic. Finally, all the excess fluid was adequately absorbed by the absorption pad at the end of the strip. After the completion of these processes, the colorimetric method was used for rapid detection, followed by Raman spectroscopy for more accurate and sensitive analysis.

3.2.2. *Specificity study of SERS-based LFIA strip*

In the bovine serum sample, a high concentration, 1 μg/mL IgM and 1 μg/mL IgG were added and the experiment was conducted according to 2.6. As shown in Fig. 3a, only the IgM sample displayed an orange-red colour at the T1 line and no colour change was observed at the T2 line. Conversely, only the IgG sample displayed an orange-red colour at the T2 line and no colour change was observed at the T1 line. Moreover, only the test lines with positive results showed strong SERS signals and no prominent SERS signal was observed from the negative test lines. In addition, all the C lines were red, regardless of the presence/absence of IgM/IgG. As the GERTs immunocomplexes on the NC membrane were invisible to the naked eye, the test lines were further characterized by SEM. Figure 3b–e shows the SEM images obtained from the coloured and uncoloured test lines. For the coloured test lines, white dotted nanoparticles were heterogeneously distributed on the multi-channel surface of the NC membrane, while on the test lines without colour development white dotted nanoparticles were hardly recognized. This indicated that the conjugates of IgM/IgG tended to combine with the corresponding coated antibody (goat anti-human IgM/IgG), while there was almost no obvious specific binding to the non-corresponding coated antibody.

Table 1
The difference between the average Raman intensity of different concentrations group and the control group in the presence of BIL/HB/TG.

Interference objects	High concentration (T1/T2)	Medium concentration (T1/T2)	Low concentration (T1/T2)
BIL	10.2 ± 7.9%	8.9 ± 2.3%	19.5 ± 11.1%
	9.8 ± 7.3%	5.4 ± 3.7%	13.2 ± 7.8%
HB	7.4 ± 8.4%	5.6% ± 4.4%	17.1 ± 13.4%
	9.7 ± 4.6%	2.6 ± 6.6%	12.2 ± 4.4%
TG	7.7 ± 5.9%	4.6 ± 2.5%	5.9 ± 12.4%
	2.5 ± 8.3%	6.9 ± 2.0%	6.3 ± 8.2%

3.2.3. *Interference study of BIL, HB and TG for simultaneous detection of IgM and IgG*

Three common components, bilirubin (BIL), hemoglobin (HB) and triglyceride (TG) present in human blood were used as interference objects to investigate the anti-interference capability of SERS-based LFIA. The concentrations of BIL, HB and TG were 6 mg/mL, 10 mg/mL and 50 mg/mL respectively, these were according to the largest threshold values of commercial performance evaluation protocols. The interference objects were individually added into three groups of serum samples that contained mixed isoconcentration antibodies with high (1000 ng/mL), medium (30 ng/mL) and low (1 ng/mL) concentrations. Moreover, each group was comprised of three parallel samples along with a control sample. The test lines were detected and the spectra were collected by a portable Raman system with a 150 μm spot size, each sample was analyzed three times at different areas and the average spectrum was obtained. Images of colorimetric results of different interference objects are shown in Fig. 4a, c, d. It can be seen that it is difficult to estimate the difference between the same concentration groups and control group through a normal inspection. Therefore, SERS

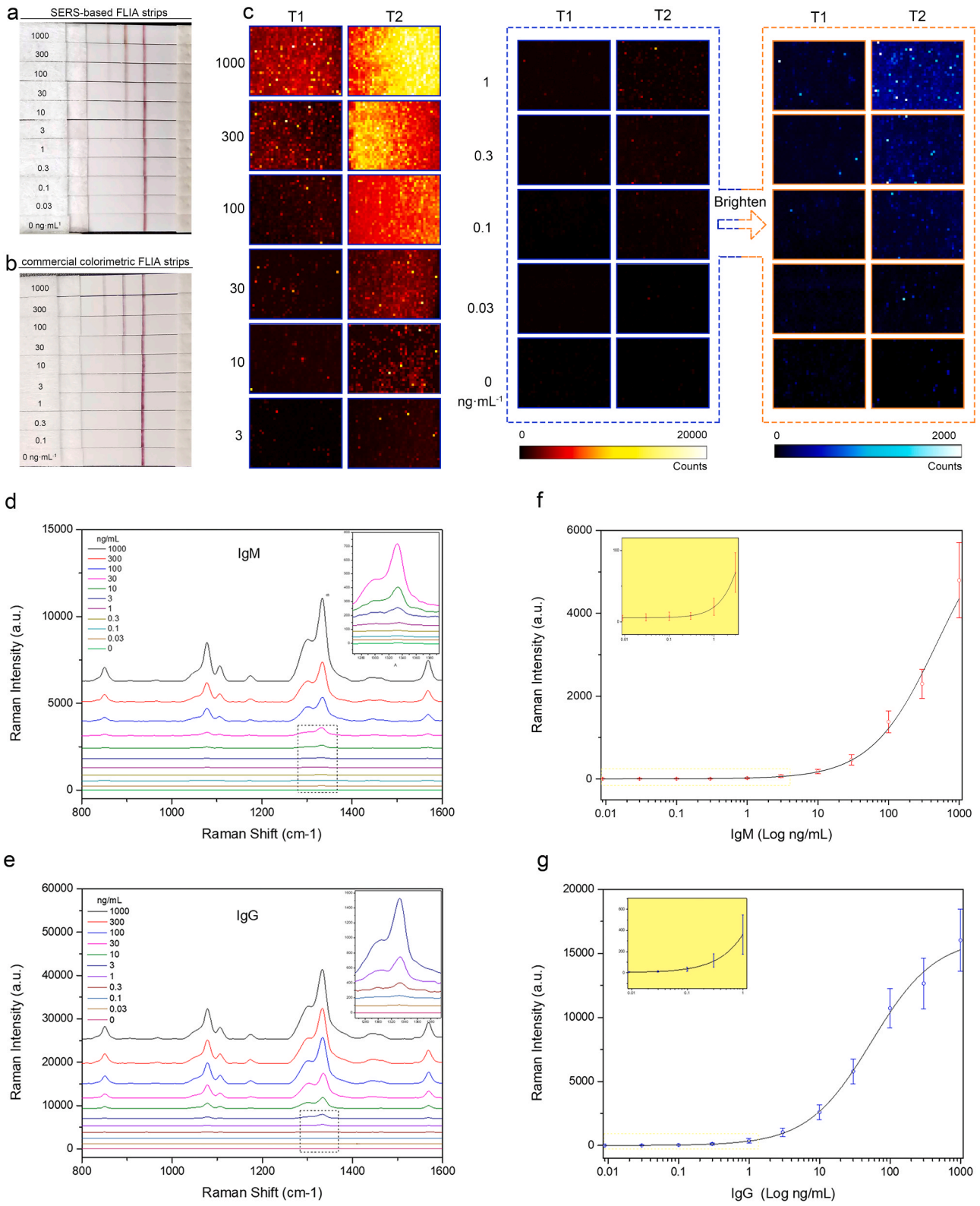

Fig. 5. (a) Photographs of SERS-based LFIA strips for IgM and IgG detection. (b) Photographs of commercial conventional LFIA strips for IgM and IgG detection. (c) SERS mapping images of the typical test zones of SERS-based LFIA strips with different concentrations of IgM and IgG. (d, e) Averaged SERS spectrum of T1 and T2 for different concentrations of IgM and IgG. (f, g) The logarithmic curve of the corresponding calibration lines for IgM and IgG. Error bars represent standard deviation ($n = 3$). All the insets show the enlarged portion of the figures.

signal acquisition method was adopted. The corresponding Raman spectrum and Raman intensity of different strips are shown in Figs. S3–5 and Fig. 4b, d, f. Then, the difference between the average Raman intensity of each concentration group and the control group in the presence of different interference objects was calculated (Table 1). For BIL, in the high, medium and low groups, the Raman intensity of T1 was 10.2 ± 7.9%, 8.9 ± 2.3%, and 19.5 ± 11.1% respectively. Raman intensity of T2 for the above-mentioned groups was 9.8 ± 7.3%, 5.4 ± 3.7%, and 13.2 ± 7.8% respectively. Similarly, for HB, the values (for the high, medium and low groups) for T1 were 7.4 ± 8.4%, 5.6% ± 4.4%, and 17.1 ± 13.4%, and for T2 79.7 ± 4.6%, 2.6 ± 6.6%, and 12.2 ± 4.4% respectively. For TG, the values for T1 were 7.7 ± 5.9%, 4.6 ± 2.5%, and 5.9 ± 12.4%, and for T2 2.5 ± 8.3%, 6.9 ± 2.0%, and 6.3 ± 8.2% respectively. These findings indicated that the interference of BIL, HB and TG to IgM and IgG is relatively low and acceptable. Hence, can be reliably applied to actual system.

3.2.4. Simultaneous qualitative and quantitative analysis of IgM and IgG

The sensitivity of the SERS-based LFIA strip to simultaneously detect IgG and IgM was investigated to meet the practical application because the majority of COVID-19 definite positive samples contain both IgM and IgG [2,7,52,53]. Different concentrations (0, 0.03, 0.1, 0.3, 1, 3, 10, 30, 100, 300, and 1000 ng/mL) of IgM and IgG mixtures with a ratio of 1:1 were added to bovine serum to simulate real samples. Figure 5a shows photos of the SERS-based LFIA of the two target antibodies. Under the optimized concentration range, the colour of the nanotags immobilized on the test lines was clearly observed with naked eye and the intensity was found to gradually decreased with decreasing antibody concentration. The limits of detection (LODs) for IgM and IgG were 10 ng/mL and 100 ng/mL, respectively. On the same strip, the colour of the T1 line was lighter than that of T2, mainly because the affinity of IgM for the recombinant antigen is weaker than that of IgG. So, less IgM were effectively bound to the nanotag and minimum number of nanotags were captured by coated antibodies. This is also the reason why the IgM detection limit was higher than that IgG. In addition, we compared the SERS-based LFIA strips with commercial LFIA strips based on 40 nm colloidal gold nanoparticles. Figure 5b shows photographs of commercial LFIA strips with different concentrations (0–1000 ng/mL) of target antibodies under the same concentration. Through colorimetric analysis, the detection limits of the commercial LFIA for IgM and IgG were consistent with those of the SERS-based LFIA, and there was an approximate colour change pattern on the test lines. The most striking difference was that the colour bands on the test lines of the commercial LFIA strips appear redder due to the characteristic resonance extinction of 40 nm gold nanoparticles near 530 nm [27]. These results indicated that the substitution of GERTs for ordinary colloidal gold nanoparticles does not affect the performance of conventional LFIAs. Figure 5c shows the SERS mapping images obtained from the test zones with the Raman intensity at 1320–1340 cm^{-1}. Each image contains 1131 (29 × 39) pixels and the intensity of the Raman signal for each pixel was represented by a pseudo-colour. A narrow-range color scale was used to brighten the pseudo-colour for low concentration of the samples. With increasing concentrations of IgM and IgG, the number of coloured pixels and brightness increased in the test zone. This was owing to the binding of more target antibodies to the nanoparticles. A higher distribution density of GERTs in the test zone led to a wider Raman signal distribution and stronger Raman signal feedback. The distribution and brightness of pixels in the test zone were heterogeneous, which was caused by the rough and porous structure on the NC membrane. Consequently, each test line was randomly measured in three zones to acquire a reproducible intensity value. Figure 5d, e shows the average SERS spectra of the three groups for different test zones. The corresponding relationship between the characteristic peak strength and logarithmic concentration is shown in Fig. 5(f-g). The error bars represent the standard deviation of the strength. For IgM, the slope was increased over the entire concentration range. For IgG, at 0–100 ng/mL, the curve

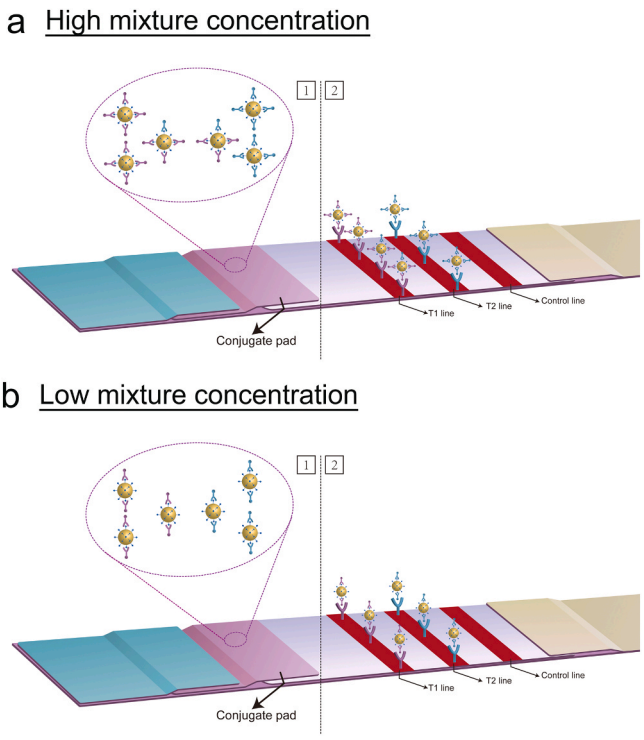

Fig. 6. (a) Schematic diagram of IgM and IgG binding to immune-GERTs in high concentration IgM/IgG mixture, and the immunobinding on T1 and T2. (b) Schematic diagram of IgM and IgG binding to immune-GERTs in low concentration IgM/IgG mixture, and the immunobinding on T1 and T2.

showed a similar upward trend as the IgM curve, while at 100–1000 ng/mL the strength slightly changed with increasing concentration. In this assay, the COVID-19 recombinant antigen containing both of the binding sites of IgM and IgG was used for immune binding. This is also a common protocol used for the multi-channel detection of IgM and IgG for COVID-19 in the current LFIA scheme [7,14–17]. However, competitive immune reactions inevitably occurred on the surface of nanotags to conjugate the same antigen. In a previous report [15], S-protein antibody was used as a single target and weaker SERS signals were observed as the S-protein concentration decreased. Then, the feasibility of quantitative analysis was confirmed and transplanted into dual-plex (IgM and IgG) detection. Here, we have a different view about this, owing to the following dynamic description obtained from the analysis of logarithmic curves. At high concentrations, because the nano-surface modified antigen can recognize both the IgM and IgG, some IgM and IgG were simultaneously bound to immune-GERTs (the physical model is shown in Fig. 6 a1) and captured by the anti-IgM antibodies in the first test line (the physical model is shown in Fig. 6 a2). This resulted in a decrease in IgG binding to the second test line and a reduction in the Raman signal growth was observed (can be seen in the right part of the curve in Fig. 5g). When the mixed antibody concentrations were gradually decreased, the immune-GERTs accordingly became excessive for IgM and IgG. Both IgM and IgG tended to be associated with their respective immune-GERTs (the physical model is shown in Fig. 6 b1) and caused a dramatic decrease in the amount of IgG transported to T1 by IgM conjugates. Namely, the IgG in the mixed system were gradually captured by T2 (the physical model is shown in Fig. 6 b2). Consequently, as shown in the left part of the curve (Fig. 5g), the IgG concentration was more positively correlated with the Raman signal intensity, which was similar to the correlation observed in the IgM curve. In conclusion, benefited from the sensitive and accurate expression of the test lines of SERS-based LFIA, the interference effect under the recognition of the same antigen was revealed through quantitative data for the first time. Obviously, this interference effect of IgM on IgG

Table 2
Performance comparison of different improved LFIA biosensors for detecting anti-SARS-CoV-2 antibodies.

References	Nanotags	Detection methods	LOD (IgM)	LOD (IgG)	Improvement factor
This work	GERTs	SERS	1 ng/mL	0.1 ng/mL	100 times sensitive than colorimetric result
Ref. [14]	Selenium nanoparticles	Colorimetry (ImageJ)	20 ng/mL	5 ng/mL	No mention
Ref. [15]	Dual-layers DTNB-modified SiO_2@Ag NPs	SERS	No mention (1 pg/mL in buffer for S-protein ab)		800 times sensitive than colorimetric result
Ref. [16]	SMNP	GMR	10 ng/mL	5 ng/mL	No mention
Ref.[17]	Dual-mode SiO2@Au@QD	Fluorescence	No mention		100 times sensitive than colorimetric result
Ref. [18]	LNPs	Fluorescence	–	No mention	No mention
Ref. [19]	PS@QDs@SiO_2 nanobeads	Fluorescence	–	No mention	More than one order of magnitude

makes it difficult to quantify IgG in the mixed system, especially at a high concentration of IgM. Therefore, using dual-plex LFIA with nanotags modified by the same antigen to quantitatively analyse the antibodies is not rigorous and reliable in multiplex detection. Hence, the dual-model quantitative analysis of the SERS-based LFIA for IgM and IgG simultaneous detection using the similar strategy [14,16,17] need to be reconsidered.

The LODs of the SERS-based LFIA strip for simultaneous detection of IgM and IgG was calculated by the following equation:

$$\mathrm{LOD} = Y_{\mathrm{blank}} + 3 \times \mathrm{SD}_{\mathrm{blank}}$$

In our experiment, Y_{blank} is the average signal intensity when the concentration is zero, and $\mathrm{SD}_{\mathrm{blank}}$ represents the standard deviation of the value measured for the blank. Thus, the LODs of IgM (1 ng/mL) and IgG (0.1 ng/mL) were easily obtained when the Raman intensity was larger than the threshold value, 17 counts. The above LODs are 100 times lower than the LODs of the colorimetric method, regardless of whether the LFIA was a SERS-based LFIA or a commercial standard LFIA. A comparison of different LFIA biosensors for anti-SARS-CoV-2 antibodies detection is listed in Table 2. Surprisingly, the reference [15] has the highest improvement factor as compared to other works, which is mainly due to the Dual-layers DTNB-modified SiO_2@Ag NPs having a signal about 220 times higher than seed NPs. This value is about seven times as compared to this research and fits well with the difference in sensitivity between the two works. Other notable differences between these two articles can be seen in Table S1. Based on the performance parameters of the above methods, SERS method has certain advantages over other methods. We look forward to more other studies and more detailed data comparisons in future work.

This improvement is important for reliable detection of infected persons with mild antibody expression, especially in the early stage of infection when IgM is difficult to detect in many cases [54] due to the poor content and relatively low specific binding ability of IgM to antigens (compared to that of IgG). As we know, a viral infection usually leads to the generation of IgM and then IgG as long-term immunity. Thus, more sensitive detection of IgM and IgG could help to obtain a more accurate determination of the date of infection and provide better guidance for treatment. Furthermore, the sensitive detection can be used to trace the source of infection which is crucial for preventing the spread of the epidemic.

4. Conclusion

In this study, we successfully prepared a novel SERS-based LFIA strip for multiplex detection of anti-SARS-CoV-2 antibodies, IgM and IgG, by using GERTs as ultra-sensitive SERS probes. The SERS signal of the GERTs was improved by 30-fold compared with that of traditional nanotags, which directly adsorbed the reporter molecules on the particle surface. Compared with colorimetric method, the LODs of the proposed SERS-based LFIA strip for simultaneous detection of IgM and IgG were decreased by two orders of magnitude to 1 ng/mL and 0.1 ng/mL respectively. The interference effect of IgM on IgG was exposed under the condition of using the same nano-surface modified antigen as a recognizer of IgM on IgG. Hence, the low sensitivity of the commercially available LFIAs will be overcome, and great potential will be exerted for IVD and POC tests for infectious diseases. With the development of Raman spectrometers, such as the line illumination probe used for a portable SERS-LFIA reader proposed by Vi Tran [55], SERS-based LFIAs are more suitable for various applications and exhibit stronger detection potential. We believe that this novel SERS-based LFIA strip will have great application prospects in in-vitro diagnosis.

CRediT authorship contribution statement

Shiliang Chen: Conceptualization, Methodology, Validation, Investigation, Writing – original draft, Writing – review & editing, Data Curation. **Liuwei Meng:** Validation, Formal analysis, Investigation, Writing – original draft, Writing – review & editing. **Litong Wang:** Validation, Formal analysis, Investigation. **Xixi Huang:** Software, Visualization, Data curation. **Shujat Ali:** Writing – original draft, Writing – review & editing. **Xiaojing Chen:** Conceptualization, Resources, Writing – review & editing, Supervision, Funding acquisition. **Mingen Yu:** Conceptualization, Methodology, Resources, Writing – review & editing. **Ming Yi:** Validation, Resources. **Limin Li:** Visualization. **Xi Chen:** Validation. **Leiming Yuan:** Visualization, Funding acquisition. **Wen Shi:** Validation. **Guangzao Huang:** Software.

Declaration of Competing Interest

The authors declare that they have no known competing financial interests or personal relationships that could have appeared to influence the work reported in this paper.

Acknowledgements

This work was supported by the Natural Science Foundation of Zhejiang [LY21C200001], National Key R&D Program of China [2017YFD0401302], Wenzhou Science and Technology Project [N20160004], Wenzhou Basic Public Welfare Project [N20190017], Zhejiang Provincial Education Department Projection [201635569] and Wenzhou Science and Technology Plan Project [G20180009].

Declaration of interest

None.

Appendix A. Supporting information

Supplementary data associated with this article can be found in the online version at doi:10.1016/j.snb.2021.130706.

References

[1] Y.J. Kim, H. Sung, C.S. Ki, M. Hur, COVID-19 testing in South Korea: current status and the need for faster diagnostics, Ann. Lab. Med. 40 (2020) 349–350.
[2] E. Sheikhzadeh, S. Eissa, A. Ismail, M. Zourob, Diagnostic techniques for COVID-19 and new developments, Talanta 220 (2020), 121392.
[3] J. Won, S. Lee, M. Park, T.Y. Kim, M.G. Park, B.Y. Choi, D. Kim, H. Chang, V. N. Kim, C.J. Lee, Development of a Laboratory-safe and Low-cost Detection

Protocol for SARS-CoV-2 of the Coronavirus Disease 2019 (COVID-19), Exp. Neurobiol. 29 (2020) 107–119.
[4] Y. Fang, H. Zhang, J. Xie, M. Lin, L. Ying, P. Pang, W. Ji, Sensitivity of chest CT for COVID-19: comparison to RT-PCR, Radiology 296 (2020) E115–E117.
[5] F. Amanat, D. Stadlbauer, S. Strohmeier, T.H.O. Nguyen, V. Chromikova, M. McMahon, K. Jiang, G.A. Arunkumar, D. Jurczyszak, J. Polanco, M. Bermudez-Gonzalez, G. Kleiner, T. Aydillo, L. Miorin, D.S. Fierer, L.A. Lugo, E.M. Kojic, J. Stoever, S. Liu, C. Cunningham-Rundles, P.L. Felgner, T. Moran, A. García-Sastre, D. Caplivski, A.C. Cheng, K. Kedzierska, O. Vapalahti, J.M. Hepojoki, V. Simon, F. Krammer, A serological assay to detect SARS-CoV-2 seroconversion in humans, Nat. Med. 26 (2020) 1033–1036.
[6] A. Velay, F. Gallais, I. Benotmane, M.J. Wendling, F. Danion, O. Collange, J. De Sèze, C. Schmidt-Mutter, F. Schneider, P. Bilbault, F. Meziani, S. Fafi-Kremer, Evaluation of the performance of SARS-CoV-2 serological tools and their positioning in COVID-19 diagnostic strategies, Diagn. Microbiol Infect. Dis. 98 (2020), 115181.
[7] Z. Li, Y. Yi, X. Luo, N. Xiong, Y. Liu, S. Li, R. Sun, Y. Wang, B. Hu, W. Chen, Y. Zhang, J. Wang, B. Huang, Y. Lin, J. Yang, W. Cai, X. Wang, J. Cheng, Z. Chen, K. Sun, W. Pan, Z. Zhan, L. Chen, F. Ye, Development and clinical application of a rapid IgM-IgG combined antibody test for SARS-CoV-2 infection diagnosis, J. Med. Virol. 92 (2020) 1518–1524.
[8] P. Brangel, A. Sobarzo, C. Parolo, B.S. Miller, P.D. Howes, S. Gelkop, J.J. Lutwama, J.M. Dye, R.A. McKendry, L. Lobel, M.M. Stevens, A serological point-of-care test for the detection of IgG antibodies against Ebola virus in human survivors, ACS Nano 12 (2018) 63–73.
[9] F. Cui, H.S. Zhou, Diagnostic methods and potential portable biosensors for coronavirus disease 2019, Biosens. Bioelectron. 165 (2020), 112349.
[10] X.L. Huang, Z.P. Aguilar, H.Y. Xu, W.H. Lai, Y.H. Xiong, Membrane-based lateral flow immunochromatographic strip with nanoparticles as reporters for detection: a review, Biosens. Bioelectron. 75 (2016) 166–180.
[11] K.M. Koczula, A. Gallotta, Lateral flow assays, Essays Biochem 60 (2016) 111–120.
[12] C. Parolo, A. Merkoci, Paper-based nanobiosensors for diagnostics, Chem. Soc. Rev. 42 (2013) 450–457.
[13] A.V. Zherdev, B.B. Dzantiev, Ways to Reach Lower Detection Limits of Lateral Flow Immunoassays, London, UK: Rapid Test - Advances in Design, Format and Diagnostic Applications. IntechOpen Limited, 2018, pp. 9–43.
[14] Z. Wang, Z. Zheng, H. Hu, Q. Zhou, W. Liu, X. Li, Z. Liu, Y. Wang, Y. Ma, A point-of-care selenium nanoparticle-based test for the combined detection of anti-SARS-CoV-2 IgM and IgG in human serum and blood, Lab. Chip. 20 (2020) 4255–4261.
[15] H. Liu, E. Dai, R. Xiao, Z. Zhou, M. Zhang, Z. Bai, Y. Shao, K. Qi, J. Tu, C. Wang, S. Wang, Development of a SERS-based lateral flow immunoassay for rapid and ultra-sensitive detection of anti-SARS-CoV-2 IgM/IgG in clinical samples, Sens. Actuators B, Chem. 329 (2021), 129196.
[16] Q. Bayin, L. Huang, C. Ren, Y. Fu, X. Ma, J. Guo, Anti-SARS-CoV-2 IgG and IgM detection with a GMR based LFIA system, Talanta 227 (2021), 122207.
[17] C. Wang, X. Yang, B. Gu, H. Liu, Z. Zhou, L. Shi, X. Cheng, S. Wang, Sensitive and simultaneous detection of SARS-CoV-2-specific IgM/IgG using lateral flow immunoassay based on dual-mode quantum dot nanobeads, Anal. Chem. 92 (2020) 15542–15549.
[18] Z. Chen, Z. Zhang, X. Zhai, Y. Li, L. Lin, H. Zhao, L. Bian, P. Li, L. Yu, Y. Wu, G. Lin, Rapid and sensitive detection of anti-SARS-CoV-2 IgG, using lanthanide-doped nanoparticles-based lateral flow immunoassay, Anal. Chem. 92 (2020) 7226–7231.
[19] C. Li, Z. Zou, H. Liu, Y. Jin, G. Li, C. Yuan, Z. Xiao, M. Jin, Synthesis of polystyrene-based fluorescent quantum dots nanolabel and its performance in H5N1 virus and SARS-CoV-2 antibody sensing, Talanta 225 (2021), 122064.
[20] Z. Wang, S. Zong, L. Wu, D. Zhu, Y. Cui, Correction to SERS-activated platforms for immunoassay: probes, encoding methods, and applications, Chem. Rev. 119 (2019) 4463.
[21] Y.Q. Wang, B. Yan, L.X. Chen, S.E.R.S. Tags, Novel optical nanoprobes for bioanalysis, Chem. Rev. 113 (2013) 1391–1428.
[22] H.H. Ye, Y.N. Liu, L. Zhan, Y.L. Liu, Z.P. Qin, Signal amplification and quantification on lateral flow assays by laser excitation of plasmonic nanomaterials, Theranostics 10 (2020) 4359–4373.
[23] C. Wang, C. Wang, X. Wang, K. Wang, Y. Zhu, Z. Rong, W. Wang, R. Xiao, S. Wang, Magnetic SERS Strip for Sensitive and Simultaneous Detection of Respiratory Viruses, ACS Appl. Mater. Interfaces 11 (2019) 19495–19505.
[24] Y. Zhang, G. Wu, J. Wei, Y. Ding, Y. Wei, Q. Liu, H. Chen, Rapid and sensitive detection of rotavirus by surface-enhanced Raman scattering immunochromatography, Mikrochim. Acta 188 (2021) 3.
[25] S. Gao, J. Wu, H. Wang, S. Hu, L. Meng, Highly sensitive detection of Cronobacter sakazakii based on immunochromatography coupled with surface-enhanced Raman scattering, J. Dairy Sci. 104 (2021) 2748–2757.
[26] S. Yan, C. Liu, S. Fang, J. Ma, J. Qiu, D. Xu, L. Li, J. Yu, D. Li, Q. Liu, SERS-based lateral flow assay combined with machine learning for highly sensitive quantitative analysis of Escherichia coli O157:H7, Anal. Bioanal. Chem. 412 (2020) 7881–7890.
[27] B.N. Khlebtsov, D.N. Bratashov, N.A. Byzova, B.B. Dzantiev, N.G. Khlebtsov, SERS-based lateral flow immunoassay of troponin I by using gap-enhanced Raman tags, Nano Res. 12 (2019) 413–420.
[28] D. Zhang, L. Huang, B. Liu, H. Ni, L. Sun, E. Su, H. Chen, Z. Gu, X. Zhao, Quantitative and ultrasensitive detection of multiplex cardiac biomarkers in lateral flow assay with core-shell SERS nanotags, Biosens. Bioelectron. 106 (2018) 204–211.
[29] X. Fu, Z. Cheng, J. Yu, P. Choo, L. Chen, J. Choo, A. SERS-based, lateral flow assay biosensor for highly sensitive detection of HIV-1 DNA, Biosens. Bioelectron. 78 (2016) 530–537.
[30] X. Fu, J. Wen, J. Li, H. Lin, Y. Liu, X. Zhuang, C. Tian, L. Chen, Highly sensitive detection of prostate cancer specific PCA3 mimic DNA using SERS-based competitive lateral flow assay, Nanoscale 11 (2019) 15530–15536.
[31] X. Liu, X. Yang, K. Li, H. Liu, R. Xiao, W. Wang, C. Wang, S. Wang, Fe_3O_4@Au SERS tags-based lateral flow assay for simultaneous detection of serum amyloid A and C-reactive protein in unprocessed blood sample, Sens. Actuators B: Chem. 320 (2020), 128350.
[32] W. Shen, C. Wang, X. Yang, C. Wang, Z. Zhou, X. Liu, R. Xiao, B. Gu, S. Wang, Synthesis of raspberry-like nanogapped Fe3O4@Au nanocomposites for SERS-based lateral flow detection of multiple tumor biomarkers, J. Mater. Chem. C 8 (2020) 12854–12864.
[33] W. Zhang, S. Tang, Y. Jin, C. Yang, L. He, J. Wang, Y. Chen, Multiplex SERS-based lateral flow immunosensor for the detection of major mycotoxins in maize utilizing dual Raman labels and triple test lines, J. Hazard. Mater. 393 (2020), 122348.
[34] N. Gandra, S.J.A.M. Singamaneni, Bilayered Raman-Intense Gold Nanostructures with Hidden Tags (BRIGHTs) for high-resolution bioimaging, Adv. Mater. 25 (2012) 1022–1027.
[35] D.K. Lim, K.S. Jeon, J.H. Hwang, H. Kim, S. Kwon, Y.D. Suh, J.M. Nam, Highly uniform and reproducible surface-enhanced Raman scattering from DNA-tailorable nanoparticles with 1-nm interior gap, Nat. Nanotechnol. 6 (2011) 452–460.
[36] B.N. Khlebtsov, N.G. Khlebtsov, Surface morphology of a gold core controls the formation of hollow or bridged nanogaps in plasmonic nanomatryoshkas and their SERS responses, J. Phys. Chem. C 120 (2016) 15385–15394.
[37] Y. Zhang, Y. Qiu, L. Lin, H. Gu, Z. Xiao, J. Ye, Ultraphotostable mesoporous silica-coated gap-enhanced Raman tags (GERTs) for high-speed bioimaging, ACS Appl. Mater. Interfaces 9 (2017) 3995–4005.
[38] N.G. Khlebtsov, L. Lin, B.N. Khlebtsov, J. Ye, Gap-enhanced Raman tags: fabrication, optical properties, and theranostic applications, Theranostics 10 (2020) 2067–2094.
[39] B. Khlebtsov, T. Pylaev, V. Khanadeev, D. Bratashov, N. Khlebtsov, Quantitative and multiplex dot-immunoassay using gap-enhanced Raman tags, RSC Adv. 7 (2017) 40834–40841.
[40] B.N. Khlebtsov, A.M. Burov, D.N. Bratashov, R.S. Tumskiy, N.G. Khlebtsov, Petal-like gap-enhanced raman tags with controllable structures for high-speed Raman imaging, Langmuir 36 (2020) 5546–5553.
[41] B. Shi, B. Zhang, Y. Zhang, Y. Gu, C. Zheng, J. Yan, W. Chen, F. Yan, J. Ye, H. Zhang, Multifunctional gap-enhanced Raman tags for preoperative and intraoperative cancer imaging, Acta Biomater. 104 (2020) 210–220.
[42] Y. Zhang, Y. Gu, J. He, B.D. Thackray, J. Ye, Ultrabright gap-enhanced Raman tags for high-speed bioimaging, Nat. Commun. 10 (2019) 3905.
[43] Y. Gu, X. Bi, J. Ye, Gap-enhanced resonance Raman tags for live-cell imaging, J. Mater. Chem. B 8 (2020) 6944–6955.
[44] Y. Gu, C. He, Y. Zhang, L. Lin, B.D. Thackray, J. Ye, Gap-enhanced Raman tags for physically unclonable anticounterfeiting labels, Nat. Commun. 11 (2020) 516.
[45] B.N. Khlebtsov, V.A. Khanadeev, A.M. Burov, N.G. Khlebtsov, A. New, Type of SERS tags: Au@Ag core/shell nanorods with embedded aromatic molecules, Nanotechnol. Russ. 12 (2017) 495–507.
[46] J.F. Li, X.D. Tian, S.B. Li, J.R. Anema, Z.L. Yang, Y. Ding, Y.F. Wu, Y.M. Zeng, Q. Z. Chen, B. Ren, Z.L. Wang, Z.Q. Tian, Surface analysis using shell-isolated nanoparticle-enhanced Raman spectroscopy, Nat. Protoc. 8 (2013) 52–65.
[47] Z.X. Ye, L. Lin, Z.Y. Tan, Y.J. Zeng, S.C. Ruan, J. Ye, Sub-100 nm multi-shell bimetallic gap-enhanced Raman tags, Appl. Surf. Sci. 487 (2019) 1058–1067.
[48] G. Frens, Controlled nucleation for the regulation of the particle size in monodisperse gold suspensions, Nat. Phys. Sci. 241 (1973) 20–22.
[49] P.N. Njoki, I.I.S. Lim, D. Mott, H.Y. Park, B. Khan, S. Mishra, R. Sujakumar, J. Luo, C.J. Zhong, Size correlation of optical and spectroscopic properties for gold nanoparticles, J. Phys. Chem. C. 111 (2007) 14664–14669.
[50] L. Lin, Q. Zhang, X. Li, M. Qiu, X. Jiang, W. Jin, H. Gu, D.Y. Lei, J. Ye, Electron transport across plasmonic molecular nanogaps interrogated with surface-enhanced Raman scattering, ACS Nano 12 (2018) 6492–6503.
[51] L. Zhang, Y. Mazouzi, M. Salmain, B. Liedberg, S. Boujday, Antibody-gold nanoparticle bioconjugates for biosensors: synthesis, characterization and selected applications, Biosens. Bioelectron. 165 (2020), 112370.
[52] D. Brigger, M.P. Horn, L.F. Pennington, A.E. Powell, D. Siegrist, B. Weber, et al., Accuracy of serological testing for SARS-CoV-2 antibodies: first results of a large mixed-method evaluation study, Allergy 00 (2020) 1–13.
[53] Q.X. Long, B.Z. Liu, H.J. Deng, G.C. Wu, K. Deng, Y.K. Chen, P. Liao, J.F. Qiu, Y. Lin, X.F. Cai, D.Q. Wang, Y. Hu, J.H. Ren, N. Tang, Y.Y. Xu, L.H. Yu, Z. Mo, F. Gong, X.L. Zhang, W.G. Tian, L. Hu, X.X. Zhang, J.L. Xiang, H.X. Du, H.W. Liu, C. H. Lang, X.H. Luo, S.B. Wu, X.P. Cui, Z. Zhou, M.M. Zhu, J. Wang, C.J. Xue, X.F. Li, L. Wang, Z.J. Li, K. Wang, C.C. Niu, Q.J. Yang, X.J. Tang, Y. Zhang, X.M. Liu, J. J. Li, D.C. Zhang, F. Zhang, P. Liu, J. Yuan, Q. Li, J.L. Hu, J. Chen, A.L. Huang, Antibody responses to SARS-CoV-2 in patients with COVID-19, Nat. Med 26 (2020) 845–848.
[54] F.J.C. González, J.M. Viuela-Prieto, J.Gd Castillo, P.B. García, M.F. Saavedra, A. H. Píriz, D.J. Virumbrales, J.C. Lebrato, G.G. de Casasola, R.G. Prieto, J.S-R. Montero, J.O. Anselmi, R.B. Martín, F.P. Roa, J.M. Martínez, A.Z. Gaviria, Utility of lateral flow tests in SARS-CoV-2 infection monitorization, Rev. Esp. Quimioter. 33 (2020) 258–266.
[55] V. Tran, B. Walkenfort, M. Konig, M. Salehi, S. Schlucker, Rapid, quantitative, and ultrasensitive point-of-care testing: a portable sers reader for lateral flow assays in clinical chemistry, Angew. Chem. Int Ed. 58 (2019) 442–446.

Shiliang Chen received B.S and M.S degrees from Fuzhou University in 2011 and 2015, respectively. He worked at Wenzhou University, Wenzhou, Zhejiang province, People's

Republic of China. His main research interests focus on application of rapid detection based on SERS technology.

Liuwei Meng received his BE degree in Animal Biotechnology from South China Agricultural University, Guangzhou, China in 2015, and ME degree in 2018 from Zhejiang University. Now, he is working at Wenzhou University. Currently, his main research interests focus on rapid detection of food quality based on spectroscopy and sensor technology.

Xiaojing Chen received Ph.D. degrees from Xiamen University in 2009. He worked at the college of Electrical and Electronic Information Engineering, Wenzhou University, Wenzhou, Zhejiang province, People's Republic of China, from June 2009. His main research interests focus on spectroscopy analysis, data mining, multivariate data analysis.